The Astrophysical Journal Letters, 816:L14 (6pp), 2016 January 1 doi:10.3847/2041-8205/816/1/L14

THE SMALL SCATTER OF THE BARYONIC TULLY–FISHER RELATION

Federico Lelli[1], Stacy S. McGaugh[1], and James M. Schombert[2]
[1] Department of Astronomy, Case Western Reserve University, Cleveland, OH 44106, USA; federico.lelli@case.edu
[2] Department of Physics, University of Oregon, Eugene, OR 97403, USA
Received 2015 October 19; accepted 2015 December 14; published 2016 January 4

ABSTRACT

In a Λ cold dark matter (ΛCDM) cosmology, the baryonic Tully–Fisher relation (BTFR) is expected to show significant intrinsic scatter resulting from the mass–concentration relation of dark matter halos and the baryonic-to-halo mass ratio. We study the BTFR using a sample of 118 disk galaxies (spirals and irregulars) with data of the highest quality: extended H I rotation curves (tracing the outer velocity) and *Spitzer* photometry at 3.6 μm (tracing the stellar mass). Assuming that the stellar mass-to-light ratio (Υ_*) is nearly constant at 3.6 μm, we find that the scatter, slope, and normalization of the BTFR systematically vary with the adopted Υ_*. The observed scatter is minimized for $\Upsilon_* \gtrsim 0.5\ M_\odot/L_\odot$, corresponding to nearly maximal disks in high-surface-brightness galaxies and BTFR slopes close to ∼4. For any reasonable value of Υ_*, the intrinsic scatter is ∼0.1 dex, below general ΛCDM expectations. The residuals show no correlations with galaxy structural parameters (radius or surface brightness), contrary to the predictions from some semi-analytic models of galaxy formation. These are fundamental issues for ΛCDM cosmology.

Key words: dark matter – galaxies: evolution – galaxies: formation – galaxies: irregular – galaxies: kinematics and dynamics – galaxies: spiral

Supporting material: data behind figure

1. INTRODUCTION

The baryonic Tully–Fisher relation (BTFR) links the rotation velocity of a galaxy to its total baryonic mass (M_b) and extends for six decades in M_b (McGaugh 2012). In a Λ cold dark matter (ΛCDM) cosmology, the BTFR must emerge from the complex process of galaxy formation, hence it is expected to show significant intrinsic scatter. Using a semi-analytic galaxy-formation model, Dutton (2012) predicts a *minimum* intrinsic scatter of ∼0.15 dex along the BTFR (see also Di Cintio & Lelli 2016). The majority of this scatter comes from the mass–concentration relation of dark matter (DM) halos, which is largely independent of baryonic processes and well-constrained by cosmological DM-only simulations (Bullock et al. 2001). Hence the BTFR scatter provides a key test for ΛCDM.

The BTFR has been extensively studied using H I observations from radio interferometers (e.g., Verheijen 2001; Noordermeer & Verheijen 2007) and single-dish telescopes (e.g., Gurovich et al. 2010; Zaritsky et al. 2014). Radio interferometers can spatially resolve the H I kinematics in nearby galaxies, providing high-quality rotation curves (RCs). Despite being limited to small galaxy samples, the study of RCs has provided key insights into the BTFR. Primarily, the BTFR scatter is minimized using the velocity along the flat part (V_f), which extends well beyond the optical galaxy (Verheijen 2001; Noordermeer & Verheijen 2007). Presumably, V_f is set by the DM halo and closely relates to its virial velocity.

Single-dish H I surveys provide large samples for BTFR studies (thousands of objects), which are most useful to estimate galaxy distances and investigate local flows (Tully et al. 2013). When interpreted in a galaxy formation context, however, they are prone to systematic effects because rotation velocities from H I line widths do not necessarily correspond to V_f (Verheijen 2001). Studies using H I line widths generally report shallower BTFR slopes (∼3) than those using V_f (∼4), leading to drastically different interpretations (Gurovich et al. 2010; McGaugh 2012). Studies based on Hα (Pizagno et al. 2007) or CO (Ho 2007) observations may present similar issues, since Hα and CO disks are typically less extended than H I disks and their maximum velocities may not be tracing V_f.

In this Letter, we investigate the BTFR using a sample of 118 galaxies with data of the highest quality: (i) extended H I RCs providing precise measurements of V_f, and (ii) *Spitzer* surface photometry at 3.6 μm providing the optimal tracer of the stellar mass.

2. DATA ANALYSIS

2.1. Galaxy Sample

This work is based on the *Spitzer* Photometry and Accurate Rotation Curves (SPARC) data set, which will be presented in detail in F. Lelli et al. (2016, in preparation). In short, we collected more than 200 high-quality H I RCs of disk galaxies from previous compilations, large surveys, and individual studies. The major sources are Swaters et al. (2009, 52 objects), Sanders & Verheijen (1998, 30 objects), de Blok & McGaugh (1997, 24 objects), Sanders (1996, 22 objects), and Noordermeer et al. (2007, 17 objects). The RCs were derived using similar techniques: fitting a tilted ring model to the H I velocity field (Begeman 1987) and/or using position–velocity diagrams along the disk major axis (de Blok & McGaugh 1997).

Subsequently, we searched the *Spitzer* archive for 3.6 μm images of these galaxies. We found 173 objects with useful [3.6] data. We derived surface brightness profiles and asymptotic magnitudes using the Archangel software (Schombert 2011), following the same procedures as Schombert & McGaugh (2014). The surface brightness profiles will be presented elsewhere; here we simply use asymptotic magnitudes at [3.6] to estimate stellar masses (M_*).

For the sake of this study, we exclude starburst dwarf galaxies (eight objects from Lelli et al. 2014a and Holmberg II from Swaters et al. 2009) because they have complex H I

kinematics and are likely involved in recent interactions (Lelli et al. 2014b). This reduces our starting sample to 164 objects.

2.2. Rotation Velocity

Empirically, the velocity along the flat part of the RC minimizes the scatter in the BTFR (Verheijen 2001). The choice of velocities at some photometric radius, like 2.2 R_d (the disk scale length; Dutton et al. 2007) or R_{80} (the radius encompassing 80% of the *i*-band light; Pizagno et al. 2007), lead to relations with larger scatter. This can be simply understood. For some low-mass, gas-dominated galaxies, these radii may occur along the rising part of the RC (Swaters et al. 2009). For high-mass, bulge-dominated galaxies, they may occur along the declining part of the RCs (Noordermeer & Verheijen 2007). These photometric radii do not necessarily imply a consistent measurement of the rotation velocity due to the different distribution of baryons within galaxies. Conversely, V_f appears insensitive to the detailed baryonic distribution, being measured at large enough radii to encompass the bulk of the baryonic mass. V_f represents our best proxy for the halo virial velocity.

We estimate V_f using a simple automated algorithm. We start by calculating the mean of the two outermost points of the RC:

$$\overline{V} = \frac{1}{2}(V_N + V_{N-1}), \quad (1)$$

and require that

$$\frac{|V_{N-2} - \overline{V}|}{\overline{V}} \leqslant 0.05. \quad (2)$$

If the condition is fulfilled, the algorithm includes V_{N-2} in the estimate of $\overline{V}$ and iterates to the next velocity point. When the condition is falsified, the algorithm returns $V_f = \overline{V}$. This algorithm returns similar values of V_f as previously employed techniques based on the logarithmic slope $\Delta \log(V)/\Delta \log(R)$ (Stark et al. 2009), but is more stable against small radial variations in the RC. Galaxies that do not satisfy the condition at the first iteration are rejected, hence we only consider RCs that are flat within ~5% over at least three velocity points. This excludes 36 galaxies with rising RCs (~20%), reducing the sample to 129 objects.

The error on V_f is estimated as

$$\delta_{V_f} = \sqrt{\frac{1}{N}\sum_i^N \delta_{V_i}^2 + \delta_{\overline{V}}^2 + \left(\frac{V_f}{\tan(i)}\delta_i\right)^2}, \quad (3)$$

where (i) δ_{V_i} is the random error on each velocity point along the flat part of the RC, quantifying non-circular motions and kinematic asymmetries between the two sides of the disk; (ii) $\delta_{\overline{V}}$ is the dispersion around $\overline{V}$, quantifying the degree of flatness of the RC; and (iii) δ_i is the error on the outer disk inclination *i*. High-quality H I velocity fields can be used to obtain kinematic estimates of *i* and trace possible warps (e.g., Battaglia et al. 2006). This is another advantage of interferometric surveys over single-dish ones, since the latter must rely on photometric inclinations that depend on the assumed stellar-disk thickness and may be inappropriate for warped H I disks. Inclination corrections become very large for face-on disks due to the $\sin(i)$ dependence, hence we exclude galaxies with $i < 30°$, reducing the sample to 118 galaxies. Clearly, this does not introduce any selection effects since galaxy disks are randomly oriented across the sky, but decreases the mean error on V_f to ~0.03 dex.

2.3. Baryonic Mass

We estimate the baryonic mass as

$$M_b = M_g + \Upsilon_* L_{[3.6]}, \quad (4)$$

where M_g is the gas mass, $L_{[3.6]}$ is the [3.6] luminosity (adopting a solar magnitude of 3.24, Oh et al. 2008), and Υ_* is the stellar mass-to-light ratio. Several studies suggest that Υ_* is almost constant in the near-infrared ([3.6] or *K*-band) over a range of galaxy types and masses. A small scatter of ~0.1 dex is consistently found using different approaches: stellar population synthesis models (McGaugh & Schombert 2014; Meidt et al. 2014), resolved stellar populations (Eskew et al. 2012), and the vertical velocity dispersion of galaxy disks (Martinsson et al. 2013). Large inconsistencies persist in the overall normalization (McGaugh & Schombert 2015). In this Letter, we assume that Υ_* is constant among galaxies and systematically explore the BTFR for different Υ_*.

In disk galaxies M_g is typically dominated by atomic gas (probed by H I observations). The molecular gas content can be estimated from CO observations assuming a CO-to-H_2 conversion factor, which can vary from galaxy to galaxy depending on metallicity or other properties. CO emission is often undetected in low-mass, metal-poor galaxies (Schruba et al. 2012). Luckily, molecules generally are a minor dynamical component, contributing less than 10% to M_b (McGaugh & Schombert 2015). Similarly, warm/hot gas is negligible in the disk (McGaugh 2012). Hence we assume $M_g = 1.33 M_{H\,I}$, where the factor 1.33 takes the contribution of helium into account. We note that any contribution from "dark gas" (molecular and/or ionized) is implicitly included in Υ_* as long as this scales with M_*.

The error on M_b is estimated as

$$\delta_{M_b} = \sqrt{\delta_{M_g}^2 + (\Upsilon_* \delta_L)^2 + (L\ \delta_{\Upsilon_*})^2 + \left(2M_b\frac{\delta_D}{D}\right)^2}, \quad (5)$$

where δ_{M_g} and δ_L are, respectively, the errors on M_g and $L_{[3.6]}$ due to uncertainties on total fluxes (generally smaller than ~10%). We assume $\delta_{\Upsilon_*} = 0.11$ dex, as suggested by stellar population models (McGaugh & Schombert 2014; Meidt et al. 2014). Galaxy distances (*D*) and corresponding errors (δ_D) deserve special attention. The 118 galaxies with accurate values of V_f have three different types of distance estimates (in order of preference):

1. Thirty-two objects have accurate distances from the tip of the red giant branch (26), Cepheids (3), or supernovae (3). These are generally on the same zero-point scale and have errors ranging from ~5% to ~10% (see Tully et al. 2013). The majority of these distances (24/32) are drawn from the Extragalactic Distance Database (Jacobs et al. 2009).
2. Twenty-six objects are in the Ursa Major cluster, which has an average distance of 18 ± 0.9 Mpc (Sorce et al. 2013). For individual galaxies, one should also consider the cluster depth (~2.3 Mpc, Verheijen 2001), hence we adopt $\delta_D = \sqrt{2.3^2 + 0.9^2} = 2.5$ Mpc, giving

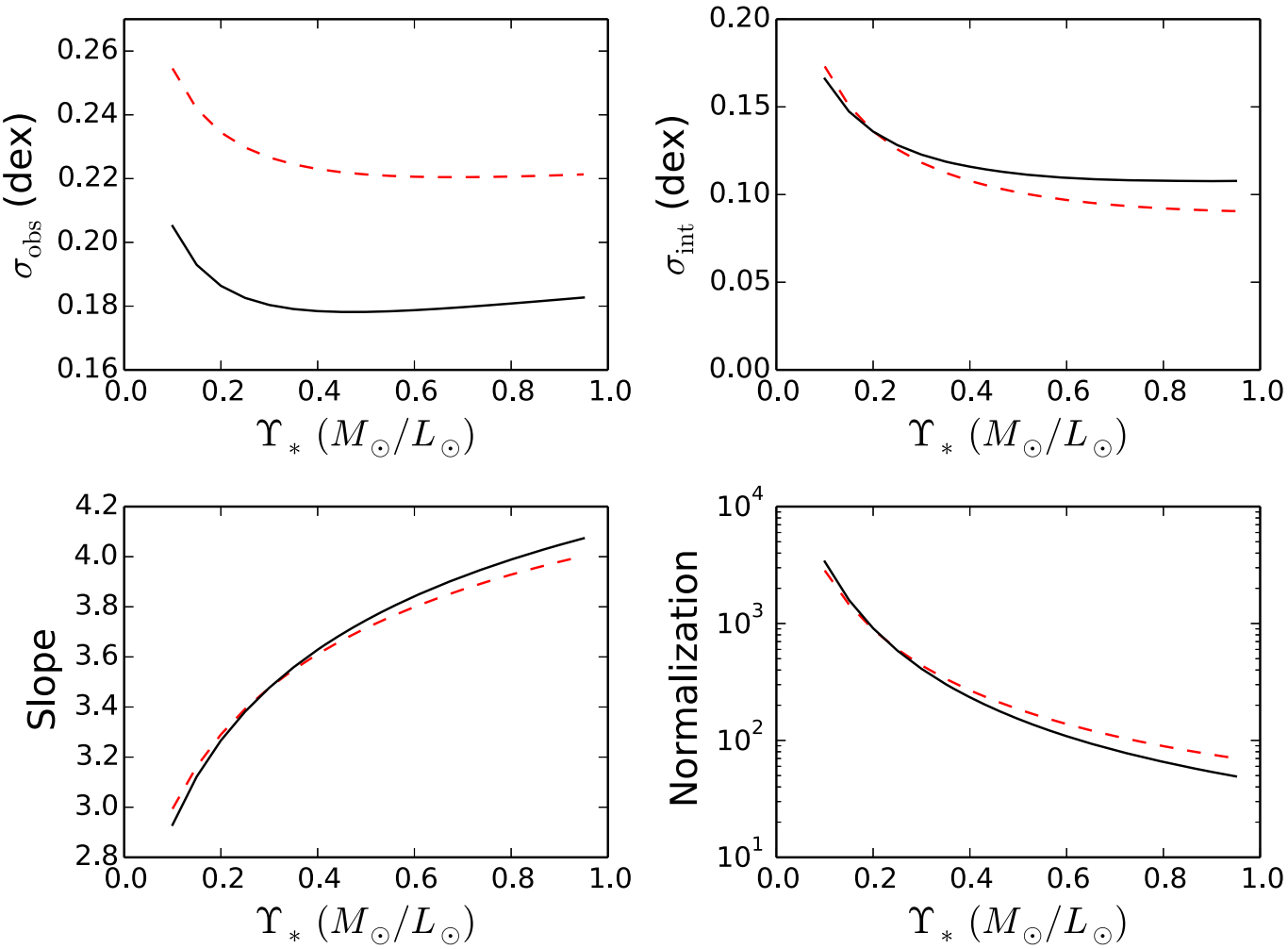

Figure 1. Properties of the BTFR as a function of Υ_*: observed scatter (top left), intrinsic scatter (top right), slope (bottom left), and normalization (bottom right). Dashed and solid lines show results for the total and accurate-distance samples, respectively.

an error of ∼14%. We consider two galaxies from Verheijen (2001) as background/foreground objects: NGC 3992, having $D \simeq 24$ Mpc from a SN Ia (Parodi et al. 2000), and UGC 6446, lying near the cluster boundary in both space and velocity ($D \simeq 12$ Mpc from the Hubble flow).

3. Sixty objects have Hubble-flow distances corrected for Virgocentric infall (as given by NED[3] assuming $H_0 = 73\,{\rm km\,s^{-1}\,Mpc^{-1}}$). These are very uncertain for nearby galaxies where peculiar velocities may constitute a large fraction of the systemic velocities, but become more accurate for distant objects. Considering that peculiar velocities may be as high as $\sim$500 km s^{-1} and H_0 has an uncertainty of ∼7%, we adopt the following errors: 30% for $D \leqslant 20$ Mpc; 25% for $20 < D \leqslant 40$ Mpc; 20% for $40 < D \leqslant 60$ Mpc; 15% for $60 < D \leqslant 80$ Mpc; and 10% for $D > 80$ Mpc. The most distant galaxy in our sample is NGC 6195 at $D \simeq 130$ Mpc.

[3] The NASA/IPAC Extragalactic Database (NED) is operated by the Jet Propulsion Laboratory, California Institute of Technology, under contract with the National Aeronautics and Space Administration.

We perform separate analyses for the total sample (mean $\delta_{M_{\rm b}} \simeq 0.2$ dex) and for galaxies with accurate distances (58 objects in groups 1 and 2; mean $\delta_{M_{\rm b}} \simeq 0.1$ dex).

3. RESULTS

We systematically explore the BTFR for different values of Υ_* ranging from 0.1 to 1.0 $M_\odot/L_\odot$ in steps of 0.05. Values higher than 1 are ruled out by maximum-disk models of high-surface-brightness (HSB) galaxies (F. Lelli et al. 2016, in preparation). For each Υ_*, we fit a straight line:

$$\log(M_{\rm b}) = s\log(V_{\rm f}) + \log(A). \quad (6)$$

We use the LTS_LINEFIT algorithm (Cappellari et al. 2013), which performs a least-square minimization considering errors in both variables and allowing for intrinsic scatter. Figure 1 shows the observed scatter ($\sigma_{\rm obs}$), intrinsic scatter ($\sigma_{\rm int}$), slope (s), and normalization (A) as a function of Υ_*.

3.1. Observed and Intrinsic Scatter

Figure 1 (top left) shows that $\sigma_{\rm obs}$ decreases with Υ_* and reaches a plateau at $\Upsilon_* \gtrsim 0.5 M_\odot/L_\odot$. This plateau actually is a broad minimum that becomes evident by extending the Υ_* range up to unphysical values of ∼10 $M_\odot/L_\odot$ (not shown). The

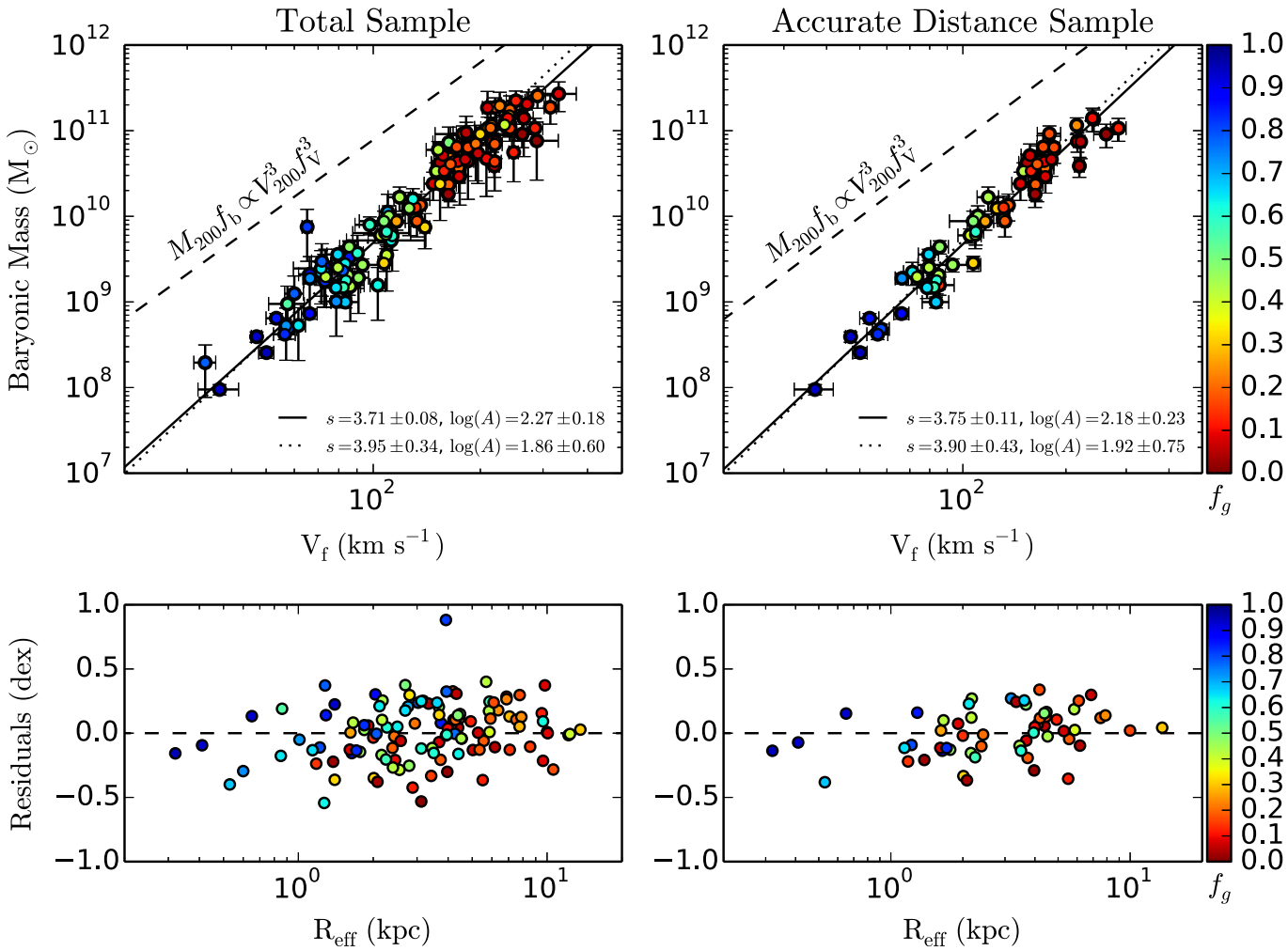

Figure 2. Top panels: BTFR adopting $\Upsilon_* = 0.5\ M_\odot/L_\odot$. Galaxies are color-coded by $f_g = M_g/M_b$. Solid lines show error-weighted fits. Dotted lines show fits weighted by f_g^2, increasing the importance of gas-dominated galaxies. The dashed line shows the ΛCDM initial condition with $f_V = 1$ and $f_b = 0.17$ (the cosmic value). Bottom panels: residuals from the error-weighted fits vs. the galaxy effective radius. The outlier is UGC 7125, which has an unusually high correction for Virgocentric infall and lies near the region where the infall solution is triple-valued. If we consider only the correction for Local Group motion, UGC 7125 lies on the BTFR within the scatter. The data for this figure are available.

observed scatter is systematically lower for the accurate-distance sample, indicating that a large portion of σ_{obs} in the full sample is driven by distance uncertainties.

Figure 1 (top right) shows that σ_{int} is below 0.15 dex for any realistic value of Υ_*. The similar intrinsic scatter between the two samples suggests that our errors on Hubble-flow distances are realistic. For a fiducial value of $\Upsilon_* = 0.5\ M_\odot/L_\odot$, we find $\sigma_{int} = 0.10 \pm 0.02$ for the full sample and $\sigma_{int} = 0.11 \pm 0.03$ for the accurate-distance sample. As we discuss in Section 4, this represents a challenge for the ΛCDM cosmological model.

3.2. Slope, Normalization, and Residuals

Figure 1 (bottom panels) shows that the BTFR slope (normalization) monotonically increases (decreases) with Υ_*. This is due to the systematic variation of the gas fraction ($f_g = M_g/M_b$) with V_f. Figure 2 (top panels) shows the BTFR for $\Upsilon_* = 0.5\ M_\odot/L_\odot$, color-coding each galaxy by f_g. Low-mass galaxies tend to be gas-dominated ($f_g \gtrsim 0.5$) and their location on the BTFR does not strongly depend on the assumed Υ_* (Stark et al. 2009; McGaugh 2012). Conversely, high-mass galaxies are star-dominated and their location on the BTFR strongly depends on Υ_*. By decreasing Υ_*, M_b decreases more significantly for high-mass galaxies than for low-mass ones, hence the slope decreases and the normalization increases.

For any Υ_*, we find no correlation between BTFR residuals and galaxy effective radius: the Pearson's, Spearman's, and Kendall's coefficients are consistently between ± 0.4. Figure 2 (bottom panels) shows the case of $\Upsilon_* = 0.5\ M_\odot/L_\odot$. Similarly, we find no trend with effective surface brightness. We have also fitted exponentials to the outer parts of the luminosity profiles and find no trend between residuals and central surface brightness or scale length. These results differ from those of Zaritsky et al. (2014) due to the use of V_f instead of H I line widths (see also Verheijen 2001). The lack of any trend between BTFR residuals and galaxy structural parameters is an issue for galaxy formation models, which generally predict such correlations (Dutton et al. 2007; Desmond & Wechsler 2015).

Gas-dominated galaxies provide an absolute calibration of the BTFR. McGaugh (2012) used 45 galaxies that were selected for having $f_g > 0.5$ (assuming Υ_* based on stellar population models). Here we use a slightly different approach: we fit the BTFR weighting each point by $1/f_g^2$. In this way, galaxies with $f_g = 0.5$ are 25 times more important in the fit than galaxies with $f_g = 0.1$. Our results are shown in Figure 2 for $\Upsilon_* = 0.5\ M_\odot/L_\odot$, using both standard error-weighted fits and f_g^2-weighted fits. The latter hints at a small, systematic increase of Υ_* with $1/f_g$ or V_f (by ∼0.1 dex) in order to have symmetric residuals.

4. DISCUSSION AND CONCLUSIONS

In this Letter we study the BTFR using 118 galaxies with data of the highest quality: extended H I RCs tracing V_f and *Spitzer* photometry at 3.6 μm tracing M_*. We systematically explore the BTFR for different values of Υ_* and find the following results:

1. The observed scatter reaches a broad minimum for $\Upsilon_* \gtrsim 0.5 M_\odot/L_\odot$, corresponding to nearly maximal stellar disks in HSB galaxies;
2. For any reasonable value of Υ_*, the intrinsic scatter is below the *minimum* value expected in a ΛCDM cosmology (0.15 dex, Dutton 2012);
3. The residuals around the BTFR show no trend with galaxy size or surface brightness, providing a further challenge to galaxy formation models (Desmond & Wechsler 2015).

In a ΛCDM cosmology, the BTFR results from an underlying correlation between the "virial" mass (M_{200}) and "virial" velocity (V_{200}) of the DM halo (Mo et al. 1998). Following McGaugh (2012), we write

$$M_{200} = (\sqrt{100}\, G\, H_0)^{-1} V_{200}^3, \quad (7)$$

where G and H_0 are Newton's and Hubble's constants, respectively. By construction, this relation has no intrinsic scatter. To map M_{200} and V_{200} onto the observed BTFR, we introduce the baryonic fraction $f_b = M_b/M_{200}$ and the factor $f_V = V_f/V_{200}$, hence

$$M_b \propto f_b f_V^{-3} V_f^3. \quad (8)$$

Since the observed BTFR has a slope higher than 3, we infer that f_b and/or f_V systematically vary with M_b. The presumed f_b–M_b and f_V–M_b relations are set by the galaxy formation process and must induce scatter on the observed BTFR. The factor f_b is determined by baryonic processes like gas inflows, reionization, stellar feedback, and gas outflows. The factor f_V, instead, is determined both by "primordial" halo properties (mass–concentration relation) and subsequent baryonic physics (halo contraction due to baryonic infall or expansion due to stellar feedback).

The mass–concentration relation has a well-established scatter of 0.11 dex from N-body simulations (Dutton & Macciò 2014), driving scatter on f_V. The M_*–M_{200} relation, proxy of a more fundamental M_b–M_{200} relation, has an estimated scatter of ∼0.1–0.2 dex (Moster et al. 2013; Zu & Mandelbaum 2015), driving scatter on f_b. Since these two sources of scatter act in perpendicular directions on the BTFR, we expect an intrinsic scatter of *at least* ∼0.15–0.2 dex. For example, Dutton (2012) uses a semi-analytic model of galaxy formation to reproduce the BTFR and predicts a minimum intrinsic scatter of 0.15 dex. In his model, most of the expected scatter (∼73%) comes from the mass–concentration relation, while the remaining fraction comes from variations in the halo spin parameter. Hence, a value of ∼0.15 is a *lower limit* for ΛCDM cosmology: it is hard to imagine that stochastic baryonic processes would conspire to reduce the scatter expected from the basic structure of DM halos. Conversely, the diverse formation histories of galaxies should lead to significant variations in f_b at a given halo mass (Eisenstein & Loeb 1996; McGaugh & de Blok 1998), hence a scatter larger than 0.15 dex would be a more natural result.

We find that the BTFR intrinsic scatter is ∼0.11 dex, below ΛCDM expectations. For galaxies with accurate distances, the observed scatter is already small (∼0.18 dex), thus there is little room for having overestimated the errors. Moreover, $\sigma_{int} \simeq 0.11$ dex is comparable to the mean error on M_b (driven by the assumed uncertainty on Υ_*), hence it should be considered as an observational *upper limit*.

One may wonder whether selection effects may artificially decrease the BTFR scatter. For example, Gurovich et al. (2010) argued that the exclusion of low-mass galaxies with rising RCs may introduce a bias toward objects where the H I distribution is more extended with respect to the DM scale length. This is hardly the case. For low-mass bulgeless galaxies, RCs start to flatten at ∼2 R_d (independently of mass or luminosity) and reach a flat part beyond ∼3 R_d (Swaters et al. 2009). The presence or not of a flat part is mostly related to our ability to trace RCs out to large radii, where the H I column densities are low and the sensitivity of the observations decreases. Hence, the exclusion of galaxies with rising RCs helps *avoid* observational bias.

We stress that our sample spans a large range in mass ($10^8 \lesssim M_b/M_\odot \lesssim 10^{11}$), size ($0.3 \lesssim R_{eff}/\mathrm{kpc} \lesssim 15$), surface brightness ($8 \lesssim \Sigma_{eff}/L_\odot\ \mathrm{pc}^{-2} \lesssim 3000$), gas fraction ($0.01 \lesssim f_g \lesssim 0.95$), and morphology (S0 to Im). We are only excluding merging and interacting galaxies, since they show disturbed, out-of-equilibrium H I kinematics that would artificially inflate the scatter on the BTFR. Hence our results are representative for the general population of non-interacting galaxies in low-density environments (field, groups, and diffuse clusters like Ursa Major).

In conclusion, the BTFR is an open issue for the current cosmological model: the stochastic process of galaxy formation needs to reproduce a global relation with little (if any) intrinsic scatter and no dependence on galaxy structural parameters.

We thank Michele Cappellari for providing LTS_LINEFIT. The work of F.L. and S.S.M. is supported by a grant from the John Templeton Foundation.

REFERENCES

Battaglia, G., Fraternali, F., Oosterloo, T., & Sancisi, R. 2006, A&A, 447, 49
Begeman, K. G. 1987, PhD thesis, Kapteyn Institute
Bullock, J. S., Kolatt, T. S., Sigad, Y., et al. 2001, MNRAS, 321, 559
Cappellari, M., Scott, N., Alatalo, K., et al. 2013, MNRAS, 432, 1709
de Blok, W. J. G., & McGaugh, S. S. 1997, MNRAS, 290, 533
Desmond, H., & Wechsler, R. H. 2015, MNRAS, 454, 322
Di Cintio, A., & Lelli, F. 2016, MNRAS, in press (arXiv:1511.06616)
Dutton, A. A. 2012, MNRAS, 424, 3123
Dutton, A. A., & Macciò, A. V. 2014, MNRAS, 441, 3359
Dutton, A. A., van den Bosch, F. C., Dekel, A., & Courteau, S. 2007, ApJ, 654, 27

Eisenstein, D. J., & Loeb, A. 1996, ApJ, 459, 432
Eskew, M., Zaritsky, D., & Meidt, S. 2012, AJ, 143, 139
Gurovich, S., Freeman, K., Jerjen, H., Staveley-Smith, L., & Puerari, I. 2010, AJ, 140, 663
Ho, L. C. 2007, ApJ, 669, 821
Jacobs, B. A., Rizzi, L., Tully, R. B., et al. 2009, AJ, 138, 332
Lelli, F., Verheijen, M., & Fraternali, F. 2014a, A&A, 566, A71
Lelli, F., Verheijen, M., & Fraternali, F. 2014b, MNRAS, 445, 1694
Martinsson, T. P. K., Verheijen, M. A. W., Westfall, K. B., et al. 2013, A&A, 557, A131
McGaugh, S. S. 2012, AJ, 143, 40
McGaugh, S. S., & de Blok, S. S. 1998, ASPC, 136, 210
McGaugh, S. S., & Schombert, J. M. 2014, AJ, 148, 77
McGaugh, S. S., & Schombert, J. M. 2015, ApJ, 802, 18
Meidt, S. E., Schinnerer, E., van de Ven, G., et al. 2014, ApJ, 788, 144
Mo, H. J., Mao, S., & White, S. D. M. 1998, MNRAS, 295, 319
Moster, B. P., Naab, T., & White, S. D. M. 2013, MNRAS, 428, 3121
Noordermeer, E., van der Hulst, J. M., Sancisi, R., Swaters, R. S., & van Albada, T. S. 2007, MNRAS, 376, 1513
Noordermeer, E., & Verheijen, M. A. W. 2007, MNRAS, 381, 1463
Oh, S.-H., de Blok, W. J. G., Walter, F., Brinks, E., & Kennicutt, R. C., Jr. 2008, AJ, 136, 2761
Parodi, B. R., Saha, A., Sandage, A., & Tammann, G. A. 2000, ApJ, 540, 634
Pizagno, J., Prada, F., Weinberg, D. H., et al. 2007, AJ, 134, 945
Sanders, R. H. 1996, ApJ, 473, 117
Sanders, R. H., & Verheijen, M. A. W. 1998, ApJ, 503, 97
Schombert, J. 2011, Astrophysics Source Code Library, record ascl:1107.011
Schombert, J. M., & McGaugh, S. 2014, PASA, 31, 11
Schruba, A., Leroy, A. K., Walter, F., et al. 2012, AJ, 143, 138
Sorce, J. G., Courtois, H. M., Tully, R. B., et al. 2013, ApJ, 765, 94
Stark, D. V., McGaugh, S. S., & Swaters, R. A. 2009, AJ, 138, 392
Swaters, R. A., Sancisi, R., van Albada, T. S., & van der Hulst, J. M. 2009, A&A, 493, 871
Tully, R. B., Courtois, H. M., & Dolphin, A. E. 2013, AJ, 146, 86
Verheijen, M. A. W. 2001, ApJ, 563, 694
Zaritsky, D., Courtois, H., Muñoz-Mateos, J.-C., et al. 2014, AJ, 147, 134
Zu, Y., & Mandelbaum, R. 2015, MNRAS, 454, 1161